

## Article

# Effect of Cation Chloride Concentration on the Dissolution Rates of Basaltic Glass and Labradorite: Application to Subsurface Carbon Storage

Kiflom G. Mesfin<sup>1,2</sup>, Domenik Wolff-Boenisch<sup>3</sup>, Sigurdur R. Gislason<sup>1</sup> and Eric H. Oelkers<sup>1,4,\*</sup> <sup>1</sup> Institute of Earth Sciences, University of Iceland, Sturlugata 7, 101 Reykjavik, Iceland<sup>2</sup> HS Orka, Svartsengi, 240 Grindavík, Iceland<sup>3</sup> School of Earth and Planetary Sciences, Curtin University, P.O. Box U1987, Perth 6845, Australia<sup>4</sup> Ali I. Al-Naimi Petroleum Engineering Research Center, KAUST, Thuwal 23955-6900, Saudi Arabia

\* Correspondence: eric.oelkers@gmail.com

**Abstract:** The steady-state dissolution rates of basaltic glass and labradorite were measured in the presence of 10 to 700 × 10<sup>-3</sup> mol·kg<sup>-1</sup> aqueous NaCl, KCl, CaCl<sub>2</sub>, and MgCl<sub>2</sub> at 25 °C. All rates were measured in mixed flow reactors, and at pH~3.6 by the addition of HCl to the reactive fluids. The steady-state basaltic glass dissolution rates, based on Si release, increased by ~0.3 log units in the presence of 10<sup>-3</sup> mol·kg<sup>-1</sup> of either CaCl<sub>2</sub> or MgCl<sub>2</sub> compared to their rates in 10<sup>-3</sup> mol·kg<sup>-1</sup> of NaCl or KCl. In contrast, the steady-state dissolution rates of labradorite decreased by ~0.4 log units in the presence of 10<sup>-3</sup> mol·kg<sup>-1</sup> of either CaCl<sub>2</sub> or MgCl<sub>2</sub> compared to their rates in 10<sup>-3</sup> mol·kg<sup>-1</sup> of NaCl or KCl. These contrasting behaviours likely reflect the varying effects of these cations on the stability of rate controlling Si-rich activated complexes on the surface of the dissolving solids. On average, the Si release rates of these solids are similar to each other and increase slightly with increasing ionic strength. As the pH of water charged with 10 to 30 bars CO<sub>2</sub> is ~3.6, the results of this study indicate that both basaltic glass and labradorite dissolution will likely be effective at increasing the pH and adding Ca to the aqueous phase in saline fluids. This observation supports potential efforts to store carbon through its mineralization in saline aquifers containing Ca-bearing feldspar and in submarine basalts.

**Keywords:** labradorite; basaltic glass; mineral carbonation; dissolution rates

**Citation:** Mesfin, K.G.; Wolff-Boenisch, D.; Gislason, S.R.; Oelkers, E.H. Effect of Cation Chloride Concentration on the Dissolution Rates of Basaltic Glass and Labradorite: Application to Subsurface Carbon Storage. *Minerals* **2023**, *13*, 682. <https://doi.org/10.3390/min13050682>

Academic Editor: Abbas Taheri

Received: 1 April 2023

Revised: 2 May 2023

Accepted: 12 May 2023

Published: 17 May 2023



**Copyright:** © 2023 by the authors. Licensee MDPI, Basel, Switzerland. This article is an open access article distributed under the terms and conditions of the Creative Commons Attribution (CC BY) license (<https://creativecommons.org/licenses/by/4.0/>).

## 1. Introduction

This study is focused on quantifying the effect of the ionic strength and the concentration of some common aqueous chloride salts on the dissolution rates of basaltic glass and Ca-rich plagioclase. The dissolution rates of these solids have received significant recent attention due to their potential use as feedstock for carbon mineral storage in the subsurface [1–27]. Notably, there have been a large number of studies reporting the measured dissolution rates of basaltic glass (e.g., [17,28–37]), as well as of Ca-rich feldspar labradorite [38–49]. These past studies have explored, in detail, the effects of temperature, the presence of aqueous organic species, pH, the distance from equilibrium, and crystallographic orientation on measured dissolution rates. The present study builds on these past efforts by measuring the dissolution rates of basaltic glass and labradorite as a function of reactive aqueous concentrations of NaCl, KCl, CaCl<sub>2</sub>, and MgCl<sub>2</sub>.

The motivation for this study is to more accurately quantify the effect of major cations on the dissolution kinetics of basaltic glass and Ca-rich plagioclase to understand the potential applicability of saline fluids in carbon mineralization efforts. Notably, carbon dioxide storage in the subsurface is increasingly being targeted for injection into saline reservoirs to preserve freshwater resources (e.g., [50–52]). Some of these efforts are aimed at injecting CO<sub>2</sub> into reactive basaltic or ultramafic rocks containing saline fluids or seawater

to enhance the long-term security of carbon storage (e.g., [53–55]). Towards the improved quantification of these efforts, the dissolution rates of basaltic glass and labradorite have been determined at steady-state, far-from-equilibrium conditions in flow through reactors at a pH of 3.6 and 25 °C and in the presence of aqueous metal chloride solutions with ionic strength values of up to  $700 \times 10^{-3} \text{ mol}\cdot\text{kg}^{-1}$ . The purpose of this study is to report on the results of these measurements and to use them to assess the effect of water salinity on subsurface mineral carbonation.

## 2. Theoretical Background

The standard state adopted in this study is that of the unit activity of pure minerals and H<sub>2</sub>O at any temperature and pressure. For aqueous species other than H<sub>2</sub>O, the standard state is the unit activity of the species in a hypothetical one molal solution referenced to infinite dilution at any temperature and pressure. All thermodynamic calculations reported in this study were performed using the geochemical modelling code, PHREEQC3 [56], together with the carbfix.dat database [57].

The dissolution rates of basaltic glass and labradorite are controlled via the detachment of metals from the surface of these solids [58]. Within the context of the Transition State Theory, surface reaction-controlled dissolution rates,  $r$ , can be considered to be the difference between the forward rate ( $r_+$ ) and the reverse rate ( $r_-$ ), such that

$$r = r_+ - r_- = r_+ \left( 1 - \frac{r_-}{r_+} \right) \quad (1)$$

Taking the law of detailed balancing into account, it can be shown that Equation (1) is equivalent to [59–63]

$$r = r_+ (1 - \exp(-A/\sigma RT)) \quad (2)$$

where  $A$  refers to the chemical affinity of the reaction,  $\sigma$  stands for Temkin's average stoichiometric number equal to the ratio of the rate of destruction of the activated or precursor complex relative to the overall rate,  $R$  designates the gas constant, and  $T$  denotes the absolute temperature. The experimental evidence suggests that the value of  $\sigma$  in Equation (2) is three for both basaltic glass and labradorite [63,64]. The form of Equation (1) is such that overall rates ( $r$ ) are equal to forward rates ( $r_+$ ) when  $A \gg \sigma RT$ . All dissolution rates in the present study were measured under far-from-equilibrium conditions, such that  $A \gg \sigma RT$ . At these conditions  $r_- \ll r_+$ , and thus,  $r \approx r_+$ .

According to the Transition State Theory applied to surface-controlled dissolution reactions, the forward rate,  $r_+$ , is proportional to the concentration of a rate-controlling surface complex, such that [65,66]:

$$r_+ = k_+ [\ominus] \quad (3)$$

where  $k_+$  refers to a rate constant, and  $[\ominus]$  denotes the concentration of the rate-controlling surface complex. Previous work on basaltic glass and plagioclases with less than ~75% Ca in their cation site ( $<An_{75}$ ) suggests that their far-from-equilibrium dissolution rates are proportional to the concentration of a Si-rich surface complex. This surface complex is formed by an Al-proton exchange reaction [32,45,63,64,66,67]. This observation leads to an equation describing basaltic glass and labradorite forward dissolution rates of the following form:

$$r_+ = k'_+ s \left( \frac{a_{\text{H}^+}^3}{a_{\text{Al}^{3+}}} \right)^n \quad (4)$$

where  $k'_+$  represents a constant rate,  $s$  refers to the specific surface area of the mineral, and  $n$  denotes an exponential factor equal to ~0.33. Monovalent and divalent cations, including Na, K, Mg, and Ca, also need to be removed from the structure of basaltic glass and labradorite to create a dissolution rate-controlling Si-rich surface complex. The degree to which these cations influence the dissolution rate of these solids, however, has yet to be

quantified. The effect of these cations on the dissolution rate of these solids is explored in detail in the present study.

The rates measured in the present study are normalized to the geometric surface areas of the basaltic glass and labradorite samples. These surface areas,  $A_{geo}$ , were calculated using [68]:

$$A_{geo} = \frac{6}{\rho \cdot d_{eff}} \quad (5)$$

where  $\rho$  refers to the density of the solid, and  $d_{eff}$  refers to the effective particle diameter. This latter term,  $d_{eff}$ , was calculated using:

$$d_{eff} = \frac{d_{max} - d_{min}}{\ln\left(\frac{d_{max}}{d_{min}}\right)} \quad (6)$$

where  $d_{max}$  and  $d_{min}$  correspond to the minimum and maximum grain sizes of the prepared powders, respectively.

### 3. Materials and Methods

#### 3.1. Solids

Basaltic glass used in this study was originally collected from Stapafell Mountain in SW Iceland. This basaltic glass has been previously used in a large number of different experimental studies (e.g., [17,20,32,36,69–75]). The chemical composition of this glass, as determined via X-ray fluorescence spectrometry, is shown in Table 1. Backscattering images obtained using a scanning electron microscope confirm that while some minor microcrystalline phases are present in this glass, they are confined within glass shards [34].

**Table 1.** Chemical composition and surface areas of the basaltic glass and labradorite used in this study.

Solid	Chemical Composition	$A_{geo}$ (m <sup>2</sup> /g)
	Normalized to 1 silicon atom	
Basaltic glass	Si <sub>1.000</sub> Al <sub>0.365</sub> Fe <sub>0.191</sub> Mn <sub>0.003</sub> Mg <sub>0.294</sub> Ca <sub>0.263</sub> Na <sub>0.081</sub> K <sub>0.008</sub> Ti <sub>0.025</sub> P <sub>0.004</sub> O <sub>3.405</sub>	0.0251
Labradorite	Si <sub>1.000</sub> Al <sub>0.684</sub> Ca <sub>0.286</sub> Na <sub>0.139</sub> K <sub>0.002</sub> Fe <sub>0.008</sub> O <sub>3.107</sub>	0.0284
	Normalized to 8 oxygen atoms	
Basaltic glass	Si <sub>2.281</sub> Al <sub>0.833</sub> Fe <sub>0.436</sub> Mn <sub>0.007</sub> Mg <sub>0.669</sub> Ca <sub>0.6</sub> Na <sub>0.184</sub> K <sub>0.019</sub> Ti <sub>0.058</sub> P <sub>0.008</sub> O <sub>8</sub>	0.0251
Labradorite	Si <sub>2.359</sub> Al <sub>1.612</sub> Ca <sub>0.674</sub> Na <sub>0.327</sub> K <sub>0.006</sub> Fe <sub>0.018</sub> O <sub>8</sub>	0.0284

The labradorite sample used in this study was collected from an anorthosite intrusion located on the Hrapsey Islands in Breidafjörður, western Iceland. This intrusion has been described in detail by Kirstmannsdóttir [76]. Its chemical composition, provided in Table 1, was determined using standard wavelength dispersive techniques using the JEOL Superprobe JSL 8200 electron microprobe located at the GET/CNRS in Toulouse, France. Analyses were performed using an acceleration voltage of 15 kV, a beam current of 15 nA, and a beam diameter of 2 µm.

Solids were first dried at room temperature for several days before being crushed in plastic bags using a plastic hammer. Solids were then further ground with an agate mortar and dry sieved to obtain the 45–125 µm size fraction. This size fraction was gravitationally settled to remove fine particles, and subsequently ultrasonically cleaned five times in acetone. The resulting powder was oven dried overnight at 60 °C. The geometric surface areas of these powders were calculated using Equations (5) and (6), taking account of the densities of basaltic glass and labradorite of 3.05 and 2.70 g cm<sup>−3</sup>, which were equal to 251 and 284 cm<sup>2</sup> g<sup>−1</sup>, respectively.

### 3.2. Reactive Fluids

Reactive inlet fluids were created by dissolving Merck/Sigma-Aldrich analytical-grade NaCl, KCl, CaCl<sub>2</sub>·2H<sub>2</sub>O, or MgCl<sub>2</sub>·6H<sub>2</sub>O in deionized Millipore™ water with ionic strengths ranging from 0.01 to 2.1 mol·kg<sup>-1</sup>. The concentration of these chloride-bearing inlet solutions was selected to cover a broad range of ionic strengths. A sufficient amount of reagent grade HCl was added to each fluid to adjust the pH to 3.6. This reactive fluid pH was selected so that it would have a similar pH to that of the likely CO<sub>2</sub>-charged injection waters and to avoid the precipitation of most secondary phases. The pH of pure water in equilibrium with 25 bars of CO<sub>2</sub> pressure at 25 °C is 3.2 [12].

### 3.3. Experimental Design

Basaltic glass and labradorite dissolution experiments were performed in mixed-flow reactors. The reactor system was similar to those used in past dissolution rate studies as illustrated in Figure 1 (c.f. [36,46]). This system consisted of 300 mL acid-washed high-density polyethylene reactors maintained at a constant temperature in a thermostat-controlled water bath. The temperature was kept constant during the experiment at 25 °C. All the reactor components were made of polyethylene to avoid corrosion. All reactors, connectors, and tubing were cleaned with 0.1 mol·kg<sup>-1</sup> HCl solution for 24 h and rinsed with Millipore™ water prior to each experiment. All outlet fluid sample bottles went through the same cleaning procedure prior to sampling to prevent contamination. These reactors were stirred using floating magnetic stir bars located on the bottom of the reactors. Stirring bars were rotated with a magnetic stirring motor located underneath the water bath. Basaltic glass and labradorite dissolution experiments were initiated by placing 4 g of cleaned powder and the selected initial reactive fluid into the reactor. The reactors were then sealed, and a Masterflex™ cartridge pump delivered the inlet fluid into the polyethylene mixed-flow reactors at a rate of 0.85–1.0 g·min<sup>-1</sup>. The reactive inlet fluids were stored in 12 L compressible plastic bags during the experiments. Inlet solutions of selected concentrations of NaCl, KCl, CaCl<sub>2</sub>, and MgCl<sub>2</sub> were sequentially pumped into the reactor. The reactor fluid passed through a 10 µm filter when it exited the reactor and was further filtered through a 0.2 µm cellulose acetate filter prior to chemical analysis. The outlet fluid pH was measured at 25 °C using a Eutech Instruments© pH meter coupled with a Eutech Instruments© electrode with 3 mol·kg<sup>-1</sup> KCl outer filling solution. The electrode was calibrated with NBS standards at pH values of 4.01 and 7, with an average error less than 0.03 pH units. Fluid samples were collected and acidified with 0.5% concentrated supra-pure HNO<sub>3</sub> prior to analysis. Si concentrations of all inlet and outlet fluids were measured with inductively coupled argon plasma using a Spectro Vision optical emission spectrometer (ICP-OES). Analytical uncertainties on ICP-OES analyses were estimated to be 3%–5% based on repeated analyses. As was the case for a number of previous mineral dissolution rate studies (e.g., [70,77,78]), the experiments in this study were performed in several distinct series on individual solid powders. At the start of each experimental series, the initial reactive fluid was injected into the reactor at a constant flow rate. The reactors were then operated for at least 48 h before the first outlet fluid sample was collected. Subsequent fluid sampling was timed to allow at least 3 residence periods to pass between each sampling. The residence time is defined as the reactor volume divided by the fluid flow rate, and it had a range of 5–6 h. A steady state was assumed when four consecutive rate determinations of Si outlet concentrations were constant, with analytical uncertainty. A steady state was usually attained after 7–8 days. After reaching a steady state with the initial NaCl-bearing fluid, the inlet fluid was replaced with KCl of the same cation concentration, and the procedure was repeated. For the attainment of this second steady state, inlet fluid was then replaced with CaCl<sub>2</sub>-bearing inlet fluid of a similar concentration, resulting in a third steady state over time. Finally, CaCl<sub>2</sub> inlet fluid was replaced with MgCl<sub>2</sub>-bearing inlet solution of a similar concentration until a fourth, and final, steady state was attained. In total, each solid was dissolved in the presence of four different cation-chloride salts during each series in the order of NaCl, KCl, CaCl<sub>2</sub>, and MgCl<sub>2</sub>. Using

several distinct salts in each series facilitated the identification of distinct effects of each of them on the measured rates.

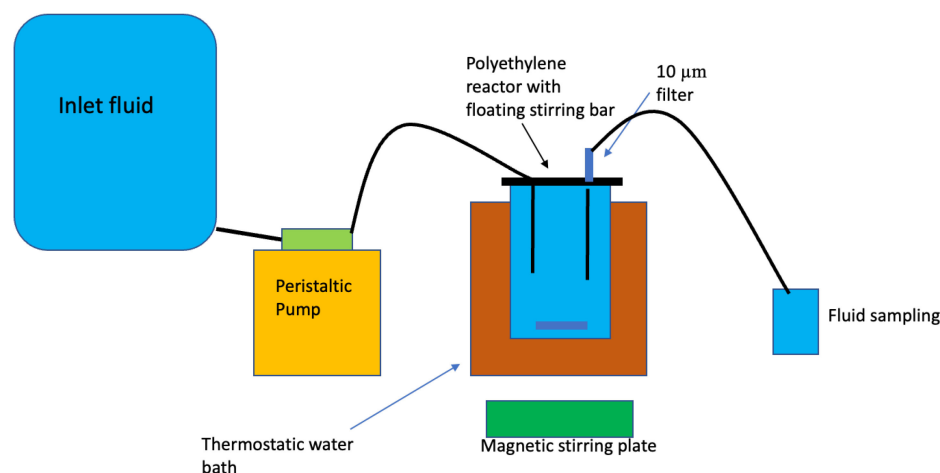


**Figure 1.** Design of the mixed-flow reactor system used to perform the experiments reported in the present study.

The basaltic glass and labradorite dissolution rates reported in this present study are based on Si release. Silicon release rates are commonly used as a measure of the dissolution rate of silicate minerals, as this metal is critical for maintaining their structure (cf. [58,63,79,80]). These rates ( $r_{\text{Si},i}$ ) were calculated from steady-state Si concentrations in the outlet fluids of the reactors using:

$$r_{\text{Si},i} = (F C_{\text{Si}}) / (v_i A_{\text{geo},i} m_i) \quad (7)$$

where  $F$  represents the fluid flow rate,  $C_{\text{Si}}$  stands for the concentration of Si in the outlet fluid at a steady state,  $v_i$  signifies the stoichiometric number of Si in one mole of the solid (1 for basaltic glass and 2.36 for labradorite),  $A_{\text{geo},i}$  denotes the specific geometric surface area of  $i$ th solid, and  $m_i$  represents the initial mass of the  $i$ th solid in the reactor.

#### 4. Results

A representative variation in the measured outlet fluid Si concentration as a function of time is shown in Figure 2. The measured Si concentrations of all samples collected during this study is provided in Table S1 of the electronic supplement. Si release rates rapidly attain a near constant value in all experiments during each reactive series, although some scatter is evident. Steady-state Si concentrations for each experiment are reported in Table 2. The integration of temporal Si release was used to estimate the total mass of solid dissolved during each experimental series. In each case, no more than 1% of the total mass of the solid was dissolved during any experiment.

Measured Si concentrations were used to determine the steady-state dissolution rate of the solids. These rates are reported in Table 2 and illustrated as a function of the concentration of each added chloride salt in Figure 3. The rates were relatively unaffected by the addition of the selected chloride salts to the reactive fluids. The geometrically measured dissolution rates vary from  $10^{-9.0}$  to  $10^{-8.3}$   $\text{mol}\cdot\text{m}^{-2}\cdot\text{s}^{-1}$  for basaltic glass and from  $10^{-9.5}$  to  $10^{-8.5}$   $\text{mol}\cdot\text{m}^{-2}\cdot\text{s}^{-1}$  for labradorite. Nevertheless, some trends are apparent. The addition of divalent metal chlorides tended to *increase* the steady-state dissolution rate of basaltic glass compared to that of the monovalent chloride salts. The steady-state basaltic glass dissolution rates measured in the presence of  $0.01 \text{ mol}\cdot\text{kg}^{-1}$  NaCl and  $0.01 \text{ mol}\cdot\text{kg}^{-1}$  KCl are approximately 0.3 orders of magnitude slower than rates measured in either  $0.01 \text{ mol}\cdot\text{kg}^{-1}$  CaCl<sub>2</sub> or MgCl<sub>2</sub>. These differences appear to decrease somewhat with increasing salt concentrations. In contrast, the addition of divalent metal chlorides tended to *decrease* the steady-state dissolution rate of labradorite more compared to that of

the monovalent chloride salts. The steady-state labradorite dissolution rates measured in the presence of  $0.01 \text{ mol}\cdot\text{kg}^{-1}$  NaCl and  $0.01 \text{ mol}\cdot\text{kg}^{-1}$  KCl are approximately 0.3 orders of magnitude slower than the rates measured in either  $0.01 \text{ mol}\cdot\text{kg}^{-1}$   $\text{CaCl}_2$  or  $\text{MgCl}_2$ . Similar to the dissolution behavior of basaltic glass, the differences in these rates appeared to decrease with an increasing salt concentration.

**Table 2.** Summary of measured steady-state dissolution rates generated in the present study. All experiments were performed under atmospheric  $P_{\text{CO}_2}$ . All inlet fluid also contained sufficient HCl to attain a pH of 3.6.

Experiment ID	Inlet Fluid Composition <sup>1</sup>	Ionic Strength ( $\text{mol}\cdot\text{kg}^{-1}$ )	Exp. Duration (h)	pH In	pH Out	(Si) Out ( $\text{mol} \times 10^5$ )	Log $r_{+\text{si}}$ Geo <sup>1</sup>
G-NaCl-10	$10 \times 10^{-3} \text{ mol}\cdot\text{kg}^{-1}$ NaCl	0.01	210	3.59	3.67	0.95	−8.85
G-KCl-10	$10 \times 10^{-3} \text{ mol}\cdot\text{kg}^{-1}$ KCl	0.01	176	3.57	3.60	0.81	−8.92
G- $\text{CaCl}_2$ -10	$10 \times 10^{-3} \text{ mol}\cdot\text{kg}^{-1}$ $\text{CaCl}_2\cdot 2\text{H}_2\text{O}$	0.03	193	3.55	3.61	1.77	−8.58
G- $\text{MgCl}_2$ -10	$10 \times 10^{-3} \text{ mol}\cdot\text{kg}^{-1}$ $\text{MgCl}_2\cdot 6\text{H}_2\text{O}$	0.03	209	3.64	3.67	2.00	−8.52
G-NaCl-100	$100 \times 10^{-3} \text{ mol}\cdot\text{kg}^{-1}$ NaCl	0.1	210	3.86	3.80	1.06	−8.80
G-KCl-100	$100 \times 10^{-3} \text{ mol}\cdot\text{kg}^{-1}$ KCl	0.1	176	3.65	3.66	0.71	−8.97
G- $\text{CaCl}_2$ -100	$100 \times 10^{-3} \text{ mol}\cdot\text{kg}^{-1}$ $\text{CaCl}_2\cdot 2\text{H}_2\text{O}$	0.3	193	3.53	3.66	1.75	−8.59
G- $\text{MgCl}_2$ -100	$100 \times 10^{-3} \text{ mol}\cdot\text{kg}^{-1}$ $\text{MgCl}_2\cdot 6\text{H}_2\text{O}$	0.3	209	3.59	3.64	1.37	−8.69
G-NaCl-700	$700 \times 10^{-3} \text{ mol}\cdot\text{kg}^{-1}$ NaCl	0.7	210	3.57	3.71	1.92	−8.55
G-KCl-700	$700 \times 10^{-3} \text{ mol}\cdot\text{kg}^{-1}$ KCl	0.7	176	3.64	3.58	1.94	−8.54
G- $\text{CaCl}_2$ -700	$700 \times 10^{-3} \text{ mol}\cdot\text{kg}^{-1}$ $\text{CaCl}_2\cdot 2\text{H}_2\text{O}$	2.1	193	3.56	3.74	3.77	−8.25
G- $\text{MgCl}_2$ -700	$700 \times 10^{-3} \text{ mol}\cdot\text{kg}^{-1}$ $\text{MgCl}_2\cdot 6\text{H}_2\text{O}$	2.1	209	3.63	3.67	1.62	−8.62
L-NaCl-10	$10 \times 10^{-3} \text{ mol}\cdot\text{kg}^{-1}$ NaCl	0.01	208	3.68	3.76	1.80	−9.02
L-KCl-10	$10 \times 10^{-3} \text{ mol}\cdot\text{kg}^{-1}$ KCl	0.01	223	3.62	3.73	1.38	−9.09
L- $\text{CaCl}_2$ -10	$10 \times 10^{-3} \text{ mol}\cdot\text{kg}^{-1}$ $\text{CaCl}_2\cdot 2\text{H}_2\text{O}$	0.03	236	3.64	3.72	0.67	−9.41
L- $\text{MgCl}_2$ -10	$10 \times 10^{-3} \text{ mol}\cdot\text{kg}^{-1}$ $\text{MgCl}_2\cdot 6\text{H}_2\text{O}$	0.03	237	3.64	3.70	0.53	−9.51
L-NaCl-50	$50 \times 10^{-3} \text{ mol}\cdot\text{kg}^{-1}$ NaCl	0.05	208	3.64	3.74	1.64	−9.03
L-KCl-50	$50 \times 10^{-3} \text{ mol}\cdot\text{kg}^{-1}$ KCl	0.05	223	3.66	3.73	1.26	−9.14
L- $\text{CaCl}_2$ -50	$50 \times 10^{-3} \text{ mol}\cdot\text{kg}^{-1}$ $\text{CaCl}_2\cdot 2\text{H}_2\text{O}$	0.15	236	3.61	3.65	0.70	−9.40
L- $\text{MgCl}_2$ -50	$50 \times 10^{-3} \text{ mol}\cdot\text{kg}^{-1}$ $\text{MgCl}_2\cdot 6\text{H}_2\text{O}$	0.15	237	3.65	3.65	0.84	−9.13
L-NaCl-200	$200 \times 10^{-3} \text{ mol}\cdot\text{kg}^{-1}$ NaCl	0.2	208	3.63	3.71	3.12	−8.75
L-KCl-200	$200 \times 10^{-3} \text{ mol}\cdot\text{kg}^{-1}$ KCl	0.2	223	3.66	3.65	3.57	−8.69
L- $\text{CaCl}_2$ -200	$200 \times 10^{-3} \text{ mol}\cdot\text{kg}^{-1}$ $\text{CaCl}_2\cdot 2\text{H}_2\text{O}$	0.6	236	3.66	3.69	2.37	−8.86
L- $\text{MgCl}_2$ -200	$200 \times 10^{-3} \text{ mol}\cdot\text{kg}^{-1}$ $\text{MgCl}_2\cdot 6\text{H}_2\text{O}$	0.6	237	3.68	3.70	1.73	−9.00

<sup>1</sup> Rates for basaltic glass are based on 1 Si per formula unit, whereas rates for labradorite are based on 2.36 Si per formula unit.

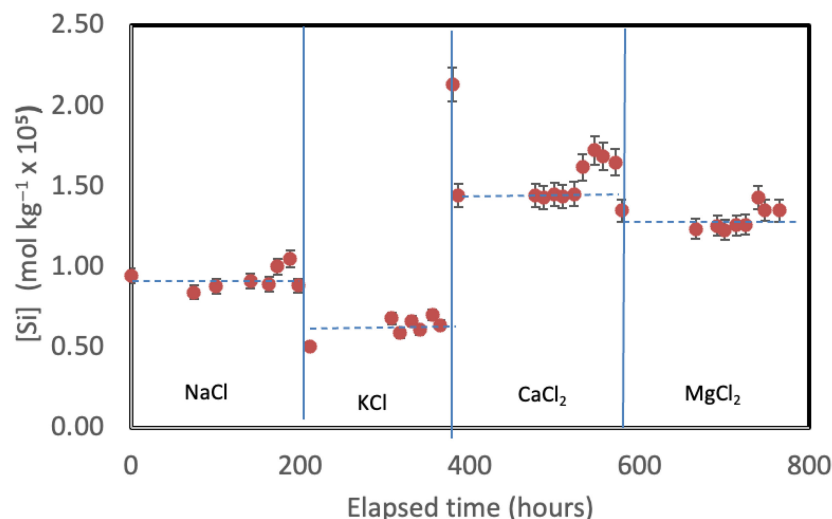


**Figure 2.** Temporal evolution of silica concentrations in the outlet fluids during basaltic glass dissolution experimental series G-100. The red symbols represent the measured Si concentration. This series consisted of a suite of four distinct experiments performed on a single basaltic glass powder, where the inlet solution composition was fixed by the addition to the aqueous inlet solution of HCl and  $0.1 \text{ mol}\cdot\text{kg}^{-1}$  of either NaCl, KCl,  $\text{CaCl}_2$ , or  $\text{MgCl}_2$ . The vertical lines denote times at which the inlet fluid was changed, whereas the dashed horizontal lines correspond to steady-state outlet Si concentrations. Where error bars are not apparent, the uncertainty of the measurement was smaller than the symbol size.

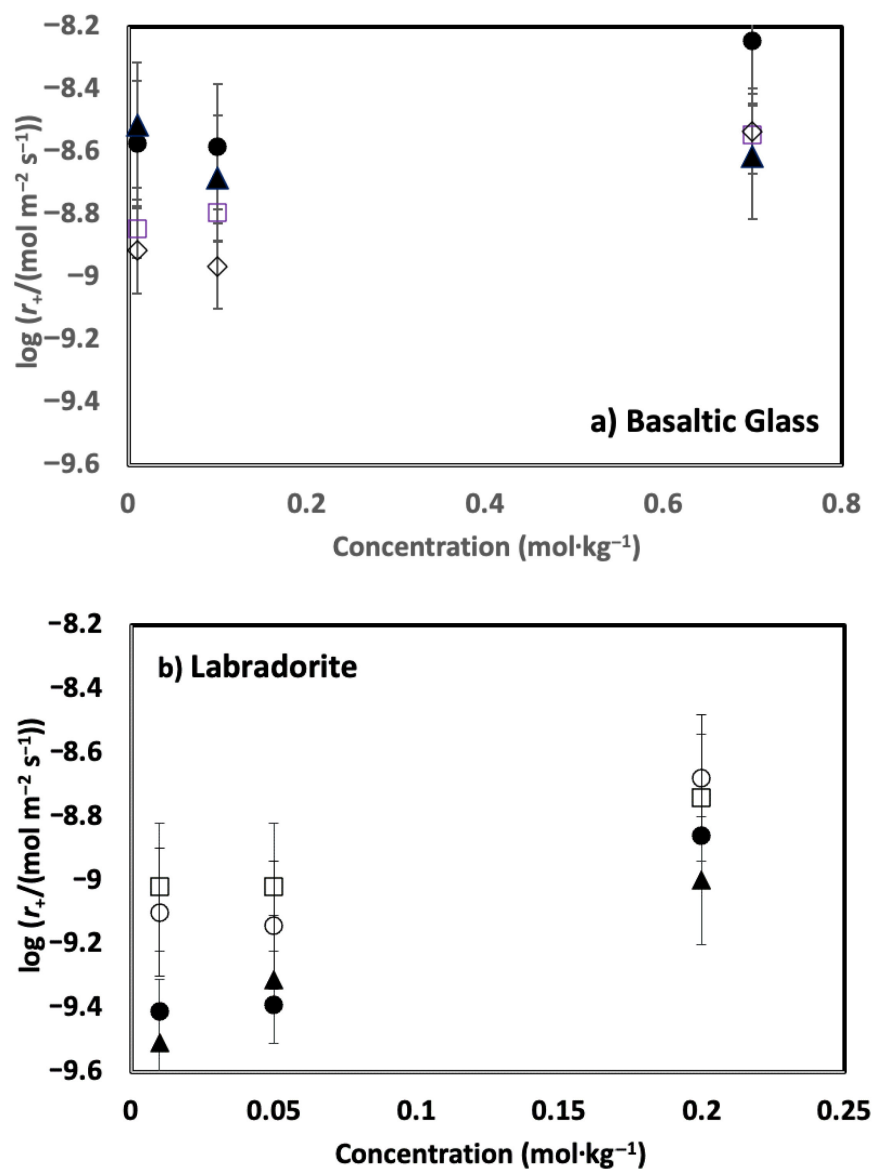


**Figure 3.** Variation in measured steady-state dissolution rates for (a) basaltic glass and (b) labradorite as a function of the concentration of salt added to the inlet fluid. The open squares, open diamonds, filled circles, and filled triangles represent rates measured in the presence of NaCl, KCl,  $\text{CaCl}_2$ , and  $\text{MgCl}_2$ , respectively.

The variation in measured steady-state rates with the ionic strength of the reactive fluid is depicted in Figure 4. The steady-state dissolution rates of both basaltic glass and labradorite increased slightly in response to the ionic strength of the reactive fluid, as indicated by the trend line in this figure. Nevertheless, a systematic scatter is evident by the variation in labradorite rates with increasing ionic strength, suggesting a small inhibitory effect of the presence of divalent metal cations on the rates.

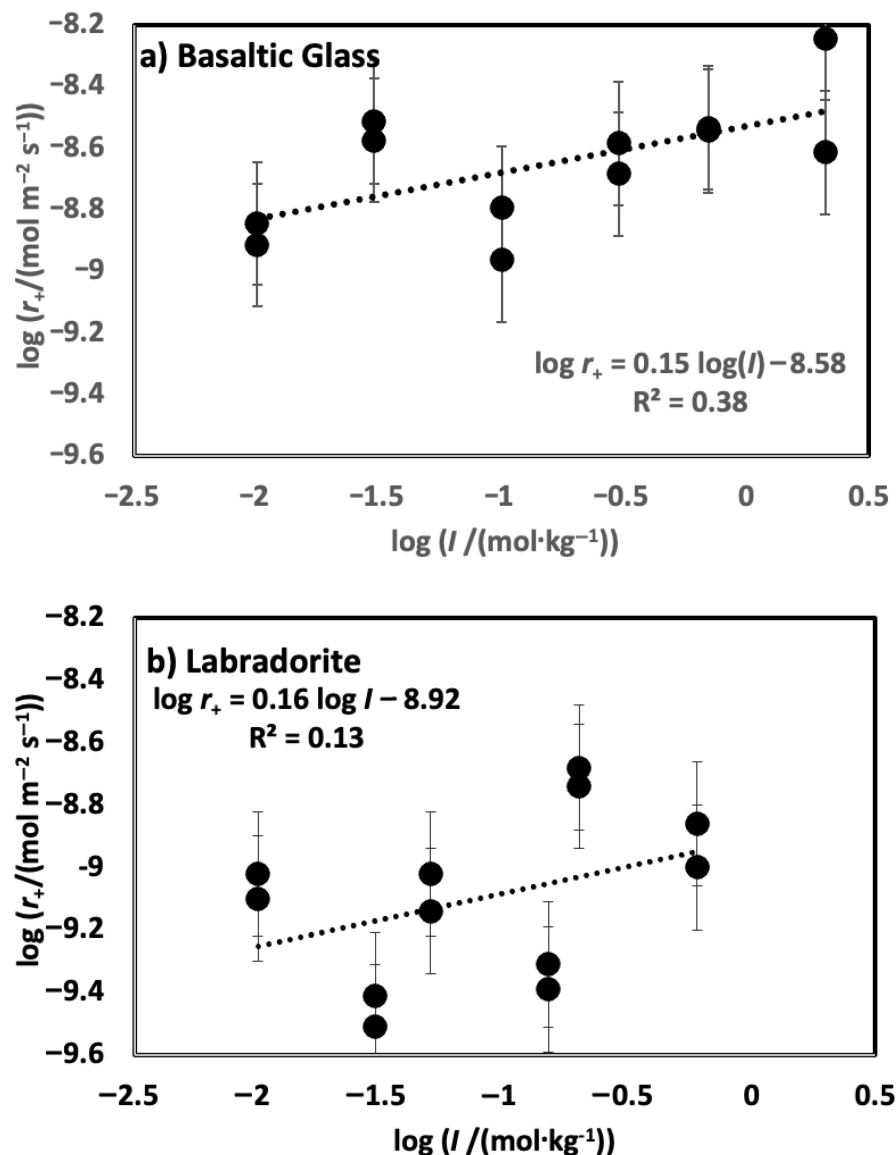


**Figure 4.** Variation in measured steady-state dissolution rates for (a) basaltic glass and (b) labradorite as a function of the logarithm of the inlet fluid ionic strength. The filled circles represent measured rates and dashed lines in this figure correspond to a least squares fit of the measured rates, where the equation of this line is provided in the figure.

## 5. Discussion

### 5.1. Comparison of Basaltic Glass and Labradorite Si Release Rates

The results of this study allow the direct comparison of the dissolution rates of basaltic glass and an intermediate feldspar. These solids are both commonly present in basaltic rocks and have similar atomic Ca/Si ratios. The atomic Ca/Si ratios of Stapafell basaltic glass and of Hrapsey Islands labradorite are 0.263 and 0.286, respectively. The availability of Ca is essential for the mineralization of CO<sub>2</sub> as solid calcium carbonate during carbon storage efforts. The measured Si release rates of these two solids are compared directly in Figure 5. As can be seen in this figure, the Si release rates of these solids are identical within uncertainty. This concurrence suggests that glassy and crystalline basalts might be equally effective at capturing and storing CO<sub>2</sub> via calcium carbonate precipitation.

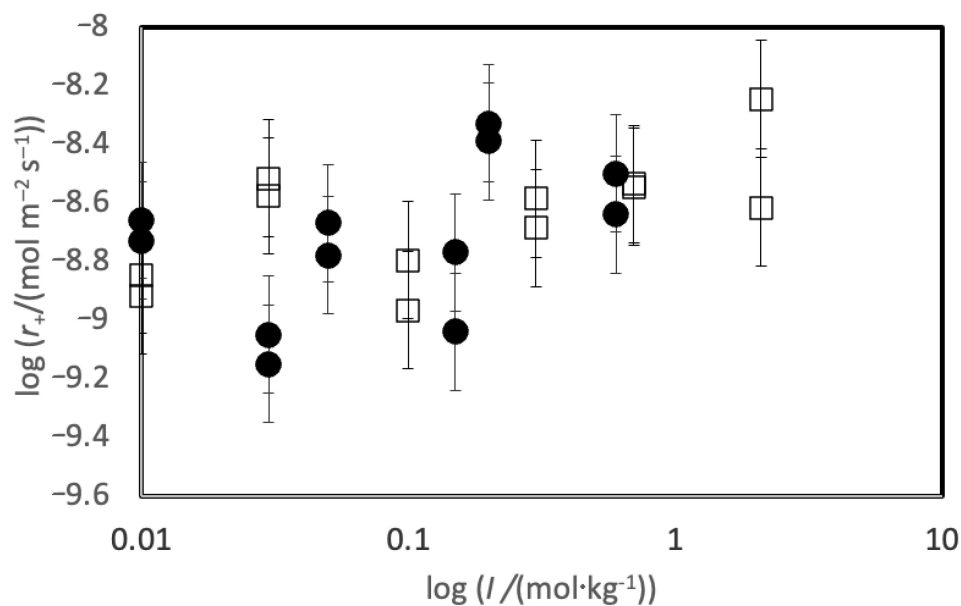


**Figure 5.** Comparison between the logarithm of the Si release rate of basaltic glass and labradorite as a function of the logarithm of ionic strength. The open squares and filled circles represent the measured dissolution rates of basaltic glass and labradorite, respectively.

### 5.2. Comparison to Previously Measured Rates

A comparison of the measured steady-state Stapafell basaltic glass dissolution rates with those of previous studies is presented in Figure 6a. This comparison is confounded by the variety of conditions and fluid compositions considered in the various experiments. Oelkers and Gislason [32] measured the dissolution rates at pH 3 and pH 11 at 25 °C in the presence of added aqueous Al, Si, and organic acids and found that the rates depended on the aqueous Al activity of the reactive fluids. Gislason and Oelkers (2003) reported the dissolution rates of Stapafell basaltic glass as a function of pH and temperature [68]. Stockmann et al. [36] measured the dissolution rates of this glass in the presence of carbonate precipitates on its surface. They found a small effect of precipitated carbonate minerals on the dissolution rates of the basaltic glass surfaces. Stockmann et al. [71] measured the dissolution rates in the presence of dead and alive bacteria and concluded that the nutrients and the presence of bacteria substantially slowed dissolution. Wolff-Boenisch et al. [17,33] reported the dissolution rates of this basaltic glass in the presence of inorganic cations, aqueous fluoride, and organic acids. They found that fluoride and aqueous organic acids substantially accelerated basaltic glass dissolution.

The rates summarized in Figure 6a suggest that the presence of increased concentrations of NaCl, KCl, CaCl<sub>2</sub>, and MgCl<sub>2</sub> do not strongly influence the rates of basaltic glass dissolution. This behavior contrasts that of aqueous Al, F, and organic acid anions. The effect of these aqueous species on basaltic glass dissolution rates were attributed to a dissolution mechanism that required the removal of aqueous Al to form the rate limiting Si-rich activated complex on the basaltic glass surface (e.g., [32,63,66]).

Gudbrandsson et al. [46] reported on the dissolution rates of labradorite samples identical to the ones considered in this study. These previous dissolution rates were measured in a mixed flow reactor system in the presence of an aqueous solution with 0.01 mol·kg<sup>-1</sup> ionic strength using NH<sub>4</sub>Cl as a background electrolyte at 22 °C. These previously reported rates are compared with those measured in the present study as a function of pH in Figure 6b. It can be seen that the rates measured in the present study are consistent with those of previous efforts. The rates of Gudbrandsson et al. [46], which were normalized to BET surface area, were recalculated to geometrically normalized dissolution rates using Equations (5) and (6) and the grain sizes reported in the original publication. The previously reported rate measured at pH = 3.76 is directly comparable to that of the

present study and equal to  $10^{-9.23} \text{ mol}\cdot\text{m}^{-2}\cdot\text{s}^{-1}$ . The rates measured at this pH and in the presence of  $0.01 \text{ mol}\cdot\text{kg}^{-1} \text{ NaCl}$  and  $0.01 \text{ mol}\cdot\text{kg}^{-1} \text{ KCl}$  in the present study are  $10^{-9.02}$  and  $10^{-9.09} \text{ mol}\cdot\text{m}^{-2}\cdot\text{s}^{-1}$ , respectively. Although these rates are similar, they suggest that the presence of Na and K in the reactive solution may have a slight accelerating effect on the rate of labradorite dissolution at this pH.

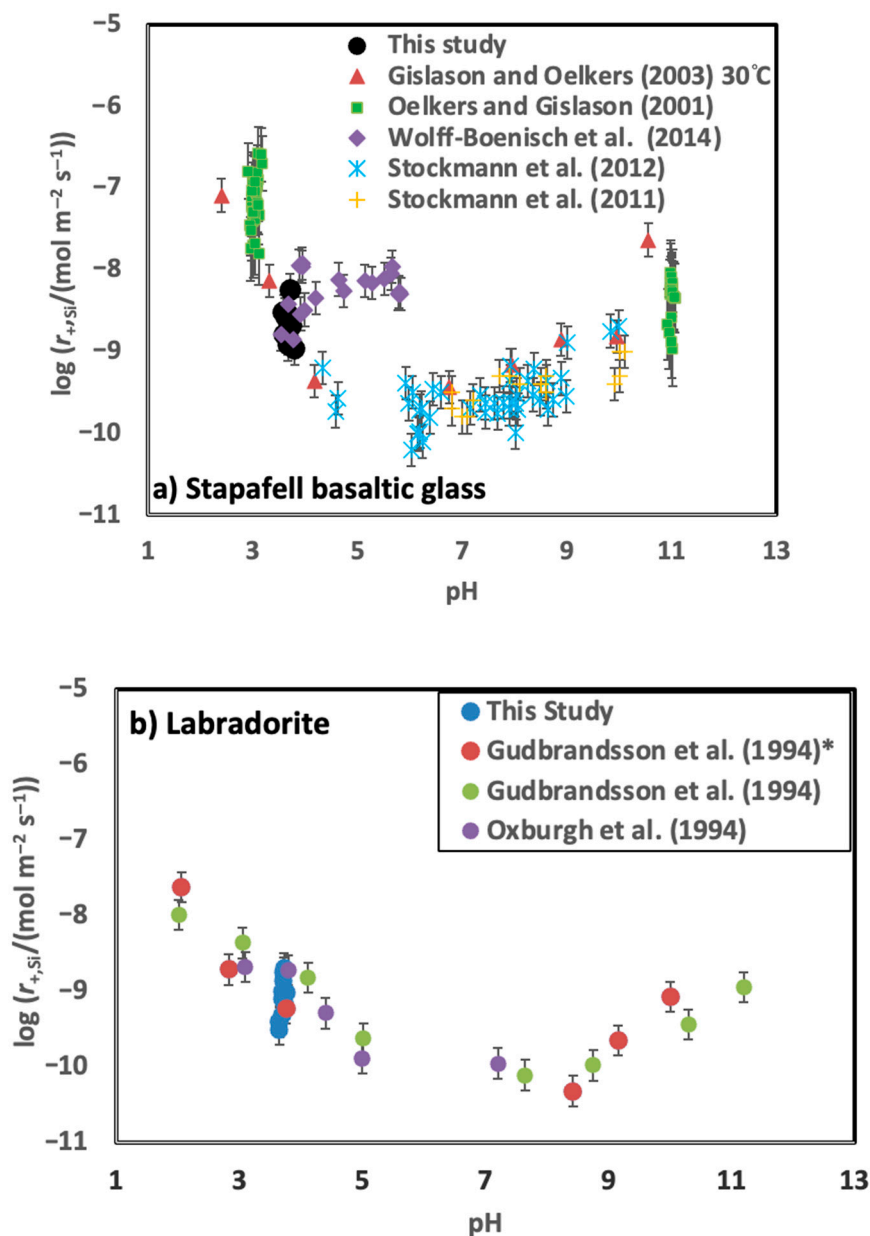


**Figure 6.** Comparison of measured geometric surface area normalized steady-state far-from-equilibrium dissolution rates measured in the present study with those reported in the literature as a function of pH at ~25 °C: (a) Stapafell basaltic glass. (b) labradorite with a composition of ~An70. The source of the data represented by the symbols are defined in the plot [17,32,46,63,71,81]. Gudbrandsson et al. [46] rates were performed using the same labradorite sample as in the present study. Error bars correspond to a 0.2 uncertainty in measured rates.

5.3. Implications for the Dissolution Mechanism of Basaltic Glass and Feldspars

Past studies have reported that the far-from-equilibrium dissolution rates of basaltic glass and feldspars having an anorthite content less than 75% slow significantly and systematically as a function of increasing aqueous aluminum activity. This observation

was attributed to the dissolution mechanism of these solids. In both cases, the dissolution rate variation in aqueous Al activity was attributed to the control of these rates by a Si-rich activated complex formed by the removal of Al from the aluminosilicate structure.

The results of the present study suggest that the presence of  $\text{CaCl}_2$  and  $\text{MgCl}_2$  decreases the labradorite dissolution rates by as much as 0.3 log units compared to the corresponding rates in the presence of aqueous NaCl and KCl solutions. This observation, which contrasts the results of Oelkers and Schott [63], suggests that these divalent metals may limit the formation of the Si-rich activated complex at the surface of Ca-rich feldspars. A potential pathway for this effect is that the presence of these divalent metals in solution may not favor the removal of divalent metals from the near surface of dissolving feldspar. This possibility could be further tested through a detailed study of the surface chemistry of Ca-rich feldspars after their interaction with compositionally distinct divalent metal-bearing fluids.

In contrast to the inhibitory effect of solute  $\text{CaCl}_2$  and  $\text{MgCl}_2$  on labradorite dissolution, these salts are observed to increase the basaltic glass dissolution rates. It seems likely that this observation is due to the role of these salts in increasing the ionic strength of aqueous solutions. This interpretation is supported by the distribution of rates illustrated in Figure 4. Basaltic glass rates appear to plot as a linear function of ionic strength. This is in contrast to the behavior of labradorite dissolution rates, which appear to plot as two distinct linear functions of ionic strength, one for monovalent and one for divalent metal chlorides. An increase in silica glass dissolution rates with increasing ionic strength was reported by Icenhower and Dove [82]; this effect was attributed to the increased charging of the mineral surface by Brady and Walther [83].

#### 5.4. Consequences for Carbon Mineral Storage in Saline Aquifers

This study considered the dissolution rates of basaltic glass and labradorite. The dissolution of these solids favor the mineralisation of  $\text{CO}_2$  via the combination of adding Ca to the aqueous phase and increasing the pH of mildly acidic waters. The results presented in this study indicate that the dissolution rates of neither basaltic glass nor labradorite are inhibited by the presence of elevated concentrations of NaCl, KCl,  $\text{CaCl}_2$ , or  $\text{MgCl}_2$  in the aqueous phase at  $\text{pH} \sim 3.5$ . In fact, the rates appeared to increase to some extent as the ionic strength of the aqueous phase increased. The pH of the reactive fluids considered in this study is similar to that of water in equilibrium with 10 to 50 bars of  $\text{CO}_2$ . It therefore seems likely that both basaltic glass and labradorite dissolution are, at least, equally able to promote the mineral storage of  $\text{CO}_2$  in saline and fresh water aquifers.

## 6. Conclusions

The rates generated in the present study indicate that the dissolution of basaltic glass and labradorite are equally efficient at releasing Ca into aqueous solution and adding alkalinity to the aqueous phase at  $\text{pH} 3.6$ . This pH is close to that expected in waters charged with  $\text{CO}_2$  at pressures from 10 to 30 bars. Notably, the dissolution rates of these minerals are found to increase mildly with increasing fluid ionic strength to as much as  $2.1 \text{ mol} \cdot \text{kg}^{-1}$ . Basaltic glass and labradorite dominate the compositions of fresh basaltic rock. Consequently, the results of this study support the likely success of mineral carbonation of fresh basaltic rocks located in saline aquifers.

**Supplementary Materials:** The following supporting information can be downloaded at: <https://www.mdpi.com/article/10.3390/min13050682/s1>, Table S1: Summary of all fluid sample measurements.

**Author Contributions:** K.G.M.: performed the experiments; D.W.-B.: designed experiments, S.R.G.: designed experiments; E.H.O.: interpreted data and wrote manuscript. All authors have read and agreed to the published version of the manuscript.

**Funding:** This project was funded by the Icelandic Science Foundation RANNÍS Geothermal Research Group GEORG 09–02–001.

**Data Availability Statement:** All data generated in this study is reported in this manuscript and its Supplementary Table S1.

**Acknowledgments:** We thank our friends and colleagues at University of Iceland, Iwona M. Galeczka, Snorri Gudbrandsson, and Eydis Eiríksdóttir, for their help during this study. EHO and SRG would like to thank Hussein A. Hoteit, and Abdulkader M. Alafifi for their hospitality while EHO and SRG stayed at KAUST University Saudi Arabia in 2023, where much of this manuscript was revised.

**Conflicts of Interest:** The authors declare no conflict of interest.

## References

1. McGrail, B.P.; Schaef, H.T.; Ho, A.M.; Chien, Y.-J.; Dooley, J.J.; Davidson, C.L. Potential for carbon dioxide sequestration in flood basalts. *J. Geophys. Res.* **2006**, *111*, B12201. [[CrossRef](#)]
2. McGrail, B.P.; Spane, F.A.; Amonette, J.E.; Thompson, C.R.; Brown, C.F. Injection and Monitoring at the Wallula Basalt Pilot Project. *Energy Procedia* **2014**, *63*, 2939–2948. [[CrossRef](#)]
3. Matter, J.M.; Takahashi, T.; Goldberg, D. Experimental evaluation of in-situ CO<sub>2</sub>–water–rock reactions during CO<sub>2</sub> injection in basaltic rocks: Implications for geological CO<sub>2</sub> sequestration. *Geochem. Geophys. Geosyst.* **2007**, *8*, Q02001. [[CrossRef](#)]
4. Matter, J.M.; Broecker, W.S.; Gislason, S.R.; Gunnlaugsson, E.; Oelkers, E.H.; Stute, M.; Sigurdardóttir, H.; Stefansson, A.; Alfreðsson, H.A.; Aradóttir, E.S.; et al. The CarbFix Pilot Project—Storing carbon dioxide in basalt. *Energy Procedia* **2011**, *4*, 5579–5585. [[CrossRef](#)]
5. Matter, J.M.; Stute, M.; Snæbjörnsdóttir, S.Ó.; Oelkers, E.H.; Gislason, S.R.; Aradóttir, E.S.; Sigfusson, B.; Gunnarsson, I.; Sigurdardóttir, H.; Gunnlaugsson, E.; et al. Rapid carbon mineralization for permanent disposal of anthropogenic carbon dioxide emissions. *Science* **2016**, *352*, 1312–1314. [[CrossRef](#)]
6. Alfreðsson, H.A.; Hardarson, B.S.; Franzson, H.; Gislason, S.R. CO<sub>2</sub> sequestration in basaltic rock at the Hellisheidi site in SW Iceland: Stratigraphy and chemical composition of the rocks at the injection site. *Min. Mag.* **2008**, *72*, 1. [[CrossRef](#)]
7. Goldberg, D.S.; Takahashi, T.; Slagel, A. Carbon dioxide sequestration in deep-sea basalt. *Proc. Nat. Acad. Sci. USA* **2008**, *105*, 9920–9925. [[CrossRef](#)]
8. Goldberg, D.S.; Slagle, A.L. A global assessment of deep-sea basalt sites for carbon storage. *Energy Proced.* **2009**, *1*, 3675–3682. [[CrossRef](#)]
9. Matter, J.M.; Kelemen, P.B. Enhanced in situ carbonation of peridotite for permanent CO<sub>2</sub> storage. *Geochim. Cosmochim. Acta* **2009**, *73*, A848.
10. Schaef, H.T.; McGrail, B.P.; Owen, A.T. Basalt–CO<sub>2</sub>–H<sub>2</sub>O interactions and variability in carbonate mineralization rates. *Energy Procedia* **2009**, *1*, 4899–4906. [[CrossRef](#)]
11. Shikazono, N.; Harada, H.; Ikeda, N.; Kashiwagi, H. Dissolution of basaltic rocks and its application to underground sequestration of CO<sub>2</sub>—Estimate of mineral trapping by dissolution–precipitation simulation. *Jpn. Mag. Mineral. Petrol. Sci.* **2009**, *38*, 149–160.
12. Gislason, S.R.; Wolff-Boenisch, D.; Stefansson, A.; Oelkers, E.H.; Gunnlaugsson, E.; Sigurdardóttir, H.; Sigfusson, B.; Broecker, W.S.; Matter, J.M.; Stute, M.; et al. Mineral sequestration of carbon dioxide in basalt: A preinjection overview of the CarbFix project. *Int. J. Greenh. Gas Control* **2010**, *4*, 537–545. [[CrossRef](#)]
13. Kampman, N.; Bickle, K.; Becker, J.; Assayag, N.; Chapman, H. Feldspar dissolution kinetics and Gibbs free energy dependence in a CO<sub>2</sub>-enriched groundwater system, Green River Utah. *Earth Planet. Sci. Lett.* **2009**, *284*, 473–488. [[CrossRef](#)]
14. Schaef, H.T.; McGrail, B.P. Dissolution of Columbia River Basalt under mildly acidic conditions as a function of temperature: Experimental results relevant to the geological sequestration of carbon dioxide. *Appl. Geochem.* **2009**, *24*, 980–987. [[CrossRef](#)]
15. Gysi, A.P.; Stefansson, A. CO<sub>2</sub>–water–basalt interaction. Numerical simulation of low temperature CO<sub>2</sub> sequestration into basalts. *Geochim. Cosmochim. Acta* **2011**, *75*, 4728–4751. [[CrossRef](#)]
16. Pham, V.T.H.; Lu, P.; Aagaard, P.; Zhu, C.; Hellevang, H. On the potential of CO<sub>2</sub>–water–rock interactions for CO<sub>2</sub> storage using a modified kinetic model. *Int. J. Greenh. Gas Contr.* **2011**, *5*, 1002–1015. [[CrossRef](#)]
17. Wolff-Boenisch, D.; Wenau, S.; Gislason, S.R.; Oelkers, E.H. Dissolution of basalts and peridotite in seawater, in the presence of ligands, and CO<sub>2</sub>: Implications for mineral sequestration of carbon dioxide. *Geochim. Cosmochim. Acta* **2011**, *75*, 5510–5525. [[CrossRef](#)]
18. Munz, I.A.; Brandvoll, Ø.; Haug, T.A.; Iden, K.; Smeets, R.; Kihle, J.; Johansen, H. Mechanisms and rates of plagioclase carbonation reactions. *Geochim. Cosmochim. Acta* **2012**, *77*, 27–51. [[CrossRef](#)]
19. Hellevang, H.; Pham, V.T.H.; Aagaard, P. Kinetic modelling of CO<sub>2</sub>–water–rock interactions. *Int. J. Greenh. Gas Control.* **2013**, *15*, 3–15. [[CrossRef](#)]
20. Wolff-Boenisch, D.; Galeczka, I.M. Flow-through reactor experiments on basalt-(sea)water-CO<sub>2</sub> reactions at 90 °C and neutral pH. What happens to the basalt pore space under post-injection conditions? *Int. J. Greenh. Gas Control* **2018**, *68*, 176–190. [[CrossRef](#)]
21. Tutolo, B.M.; Aaolayo, A.; Brown, C. Alkalinity generation constraints on basalt carbonation for carbon dioxide removal at the gigaton-per-year scale. *Environ. Sci. Technol.* **2021**, *55*, 11906–11915. [[CrossRef](#)]
22. Snæbjörnsdóttir, S.Ó.; Gislason, S.R.; Galeczka, I.M.; Oelkers, E.H. Reaction path modelling of in-situ mineralisation of CO<sub>2</sub> at the CarbFix site at Hellisheidi, SW-Iceland. *Geochim. Cosmochim. Acta* **2018**, *220*, 348–366. [[CrossRef](#)]

23. Snæbjörnsdóttir, S.Ó.; Sigfússon, B.; Marieni, C.; Goldberg, D.; Gislason, S.R.; Oelkers, E.H. Carbon dioxide storage through mineral carbonation. *Nat. Rev. Earth Environ.* **2020**, *1*, 90–102. [[CrossRef](#)]
24. Kelemen, P.B.; Benson, S.M.; Pilorge, H.; Psarras, P.; Wilcox, J. An overview of the status and challenges of CO<sub>2</sub> storage in minerals and geological formations. *Front. Clim.* **2019**, *1*, 9. [[CrossRef](#)]
25. Kelemen, P.B.; McQueen, N.; Wilcox, J.; Renforth, P.; Dipple, G.; Vankeuren, A.P. Engineered carbon mineralization in ultramafic rocks for CO<sub>2</sub> removal from air: Review and new insights. *Chem. Geol.* **2020**, *550*, 119628. [[CrossRef](#)]
26. Galeczka, I.M.; Stefánsson, A.; Kleine, B.I.; Gunnarsson-Robin, J.; Snæbjörnsdóttir, S.Ó.; Sigfússon, B.; Gunnarsdóttir, S.H.; Weisenberger, T.B.; Oelkers, E.H. A pre-injection assessment of CO<sub>2</sub> and H<sub>2</sub>S mineralization reactions at the Nesjavellir (Iceland) geothermal storage site. *Int. J. Greenh. Gas Control* **2022**, *115*, 103610. [[CrossRef](#)]
27. Oelkers, E.H.; Gislason, S.R.; Kelemen, P.B. Moving Subsurface Carbon Mineral Storage Forward. *Carbon Capture Sci. Tech.* **2023**, *7*, 100098. [[CrossRef](#)]
28. Crovisier, J.L.; Fritz, B.; Grambow, B.; Eberhart, J.P. Dissolution of basaltic glass in seawater: Experiments and thermodynamic modelling. *MRS Online Proc. Libr.* **1985**, *50*, 273–282. [[CrossRef](#)]
29. Crovisier, J.L.; Honnorez, J.; Eberhart, J.P. Dissolution of basaltic glass in seawater: Mechanism and rate. *Geochim. Cosmochim. Acta* **1987**, *51*, 2977–2990. [[CrossRef](#)]
30. Gislason, S.R.; Eugster, H.P. Meteoric water-basalt interactions: I. A laboratory study. *Geochim. Cosmochim. Acta* **1987**, *51*, 2827–2840. [[CrossRef](#)]
31. Guy, C. *Mécanismes de Dissolution des Solides Dans les Solutions Hydrothermales Deducits du Comportement des Verres Basaltiques et de Calcites Déformées*; Université Paul Sabatier: Toulouse, France, 1989.
32. Oelkers, E.H.; Gislason, S.R. The mechanism, rates and consequences of basaltic glass dissolution: I. An experimental study of the dissolution rates of basaltic glass as a function of aqueous Al, Si and oxalic acid concentration at 25 °C and pH = 3 and 11. *Geochim. Cosmochim. Acta* **2001**, *65*, 3671–3681. [[CrossRef](#)]
33. Wolff-Boenisch, D.; Gislason, S.R.; Oelkers, E.H. The effect of fluoride on the dissolution rates of natural glasses at pH 4 and 25 °C. *Geochim. Cosmochim. Acta* **2004**, *68*, 4571–4582. [[CrossRef](#)]
34. Wolff-Boenisch, D.; Gislason, S.R.; Oelkers, E.H.; Putnis, C.V. The dissolution rates of natural glasses as a function of their composition at pH 4 and 10.6, and temperatures from 25 to 74 °C. *Geochim. Cosmochim. Acta* **2004**, *68*, 4843–4858. [[CrossRef](#)]
35. Wolff-Boenisch, D.; Gislason, S.R.; Oelkers, E.H. The effect of crystallinity on dissolution rates and CO<sub>2</sub> consumption capacity of silicates. *Geochim. Cosmochim. Acta* **2006**, *70*, 858–870. [[CrossRef](#)]
36. Stockmann, G.J.; Wolff-Boenisch, D.; Gislason, S.R.; Oelkers, E.H. Do carbonate precipitates affect dissolution kinetics? 1: Basaltic glass. *Chem. Geol.* **2011**, *284*, 306–316. [[CrossRef](#)]
37. Parruzot, B.; Jollivet, P.; Rebiscoul, D.; Gin, S. Long-term alteration of basaltic glass: Mechanisms and rates. *Geochim. Cosmochim. Acta* **2015**, *154*, 28–48. [[CrossRef](#)]
38. Sjöberg, L. The effect of pH and phthalic acid on labradorite dissolution kinetics. *Geol. Föreningen I Stockh. Förhandlingar* **1985**, *107*, 311–313. [[CrossRef](#)]
39. Casey, W.H.; Westrich, H.R.; Arnold, G.W. Surface chemistry of labradorite feldspar reacted with aqueous solutions at pH 2, 3, and 12. *Geochim. Cosmochim. Acta* **1988**, *52*, 2795–2807. [[CrossRef](#)]
40. Casey, W.H.; Westrich, H.R.; Arnold, G.W.; Banfield, J.F. The surface chemistry of dissolving labradorite feldspar. *Geochim. Cosmochim. Acta* **1989**, *53*, 821–832. [[CrossRef](#)]
41. Cygan, R.T.; Casey, W.H.; Boslough, M.B.; Westrich, H.R.; Carr, M.J.; Holdren, G.R., Jr. Dissolution kinetics of experimentally shocked silicate minerals. *Chem. Geol.* **1989**, *78*, 229–244. [[CrossRef](#)]
42. Nesbitt, H.; Macrae, N.; Shoty, W. Congruent and incongruent dissolution of labradorite in dilute, acidic, salt solutions. *J. Geol.* **1991**, *99*, 429–442. [[CrossRef](#)]
43. Welch, S.A.; Ullman, W.J. Feldspar dissolution in acidic and organic solutions. Compositional and pH dependence of dissolution rate. *Geochim. Cosmochim. Acta* **1996**, *60*, 2939–2948. [[CrossRef](#)]
44. Taylor, A.S.; Blum, J.D.; Lasaga, A.C. The dependence of labradorite dissolution and Sr isotope release rates on solution saturation state. *Geochim. Cosmochim. Acta* **2000**, *64*, 2389–2400. [[CrossRef](#)]
45. Carroll, S.A.; Knauss, K.G. Dependence of labradorite dissolution kinetics on CO<sub>2</sub>(aq), Al(aq), and temperature. *Chem. Geol.* **2005**, *217*, 213–225. [[CrossRef](#)]
46. Gudbrandsson, S.; Wolff-Boenisch, D.; Gislason, S.R.; Oelkers, E.H. Experimental determination of plagioclase dissolution rates as a function of its composition and pH at 22 °C. *Geochim. Cosmochim. Acta* **2014**, *139*, 154–172. [[CrossRef](#)]
47. Wild, B.; Daval, D.; Guyot, F.; Knauss, K.G.; Pollet-Villard, M.; Imfeld, G. pH-dependent control of feldspar dissolution rate by altered surface layers. *Chem. Geol.* **2016**, *442*, 148–159. [[CrossRef](#)]
48. Gadikota, G.; Matter, J.; Kelemen, P.; Brady, P.V.; Park, A.-H. Elucidating the differences in the carbon mineralization behaviours of calcium and magnesium bearing aluminosilicates and magnesium silicates for CO<sub>2</sub> storage. *Fuel* **2020**, *277*, 117900. [[CrossRef](#)]
49. de Obeso, J.C.; Awolayo, A.N.; Nightingale, M.J.; Tan, C.; Tutolo, B.M. Experimental study on plagioclase dissolution rates at conditions relevant to mineral carbonation of seafloor basalts. *Chem. Geol.* **2023**, *620*, 121348. [[CrossRef](#)]
50. Celia, M.A.; Bachu, S.; Nordbotten, J.M.; Bandilla, K.W. Status of CO<sub>2</sub> storage in deep saline aquifers with emphasis on modeling approaches and practical simulations. *Water Resour. Res.* **2015**, *51*, 6846–6892. [[CrossRef](#)]

51. Kumar, S.; Foroozesh, J.; Edlmann, K.; Rezk, M.G.; Lim, C.Y. A comprehensive review of value-added CO<sub>2</sub> sequestration in subsurface saline aquifers. *J. Nat. Gas Sci. Eng.* **2020**, *81*, 103437. [[CrossRef](#)]
52. Ringrose, P.S.; Furre, A.-K.; Gilfillan, S.M.V.; Krevor, S.; Landrø, M.; Leslie, R.; Meckel, T.; Nazarian, B.; Zahid, A. Storage of carbon dioxide in saline aquifers: Physicochemical processes, key constraints, and scale-up potential. *Ann. Rev. Chem. Biomol.* **2021**, *12*, 471–494. [[CrossRef](#)] [[PubMed](#)]
53. Luo, S.; Xu, R.; Jiang, P. Effect of reactive surface area of minerals on mineralization trapping of CO<sub>2</sub> in saline aquifers. *Pet. Sci.* **2012**, *9*, 400–407. [[CrossRef](#)]
54. Marieni, C.; Voigt, M.; Clark, D.E.; Gislason, S.R.; Oelkers, E.H. Mineralization potential of water-dissolved CO<sub>2</sub> and H<sub>2</sub>S injected into basalts as function of temperature: Freshwater versus Seawater. *Int. J. Greenh. Gas Control* **2021**, *109*, 103357. [[CrossRef](#)]
55. Voigt, M.; Marieni, C.; Baldermann, A.; Galeczka, I.M.; Wolff-Boenisch, D.; Oelkers, E.H.; Gislason, S.R. An experimental study of basalt–seawater–CO<sub>2</sub> interaction at 130 °C. *Geochim. Cosmochim. Acta* **2021**, *308*, 21–41. [[CrossRef](#)]
56. Parkhurst, D.L.; Appelo, C.A.J. Description of Input and Examples for PHREEQC Version 3—A Computer Program for Speciation, Batch-Reaction, One-Dimensional Transport, and Inverse Geochemical Calculations. *US Geol. Surv. Tech. Methods* **2013**, *6*, 497.
57. Voigt, M.; Marieni, C.; Clark, D.E.; Gislason, S.R.; Oelkers, E.H. Evaluation and refinement of thermodynamic databases for mineral carbonation. *Energy Procedia* **2018**, *146*, 81–91. [[CrossRef](#)]
58. Brantley, S.L.; Kubicki, J.; White, A. (Eds.) *Kinetics of Water-Rock Interaction*; Springer: New York, NY, USA, 2008; 833p.
59. Aagaard, P.; Helgeson, H.C. Thermodynamic and kinetic constraints on the dissolution of feldspars. *Geol. Soc. Am. Abstr. Progr.* **1977**, *9*, 873.
60. Aagaard, P.; Helgeson, H.C. Thermodynamic and kinetic constraints on reaction-rates among minerals and aqueous-solutions. 1. Theoretical Considerations. *Am. J. Sci.* **1982**, *282*, 237–285. [[CrossRef](#)]
61. Lasaga, A.C. Transition state theory. *Rev. Min.* **1981**, *8*, 135–169.
62. Schott, J.; Oelkers, E.H. Dissolution and crystallization rates of silicate minerals as a function of chemical affinity. *Pure Appl. Chem.* **1995**, *67*, 903–910. [[CrossRef](#)]
63. Oelkers, E.H. General kinetic description of multioxide silicate mineral and glass dissolution. *Geochim. Cosmochim. Acta* **2001**, *65*, 3703–3719. [[CrossRef](#)]
64. Oelkers, E.H.; Schott, J.; Devidal, J.-L. The effect of aluminium, pH, and chemical affinity on the rates of aluminosilicate dissolution reactions. *Geochim. Cosmochim. Acta* **1994**, *58*, 2011–2024. [[CrossRef](#)]
65. Eyring, H. The activated complex in chemical reactions. *J. Chem. Phys.* **1935**, *3*, 107. [[CrossRef](#)]
66. Schott, J.; Pokrovsky, O.S.; Oelkers, E.H. The link between mineral dissolution/precipitation kinetics and solution chemistry. *Rev. Mineral. Geochem.* **2009**, *70*, 207–258. [[CrossRef](#)]
67. Oelkers, E.H.; Schott, J. Experimental study of anorthite dissolution and the relative mechanism of feldspar hydrolysis. *Geochim. Cosmochim. Acta* **1995**, *59*, 5039–5053. [[CrossRef](#)]
68. Tester, J.W.; Worley, W.G.; Robinson, B.A.; Grigsby, C.O.; Feerer, J.L. Correlating quartz dissolution kinetics in pure water from 25 to 625 °C. *Geochim. Cosmochim. Acta* **1994**, *58*, 2407–2420. [[CrossRef](#)]
69. Gislason, S.R.; Oelkers, E.H. Mechanism, rates, and consequences of basaltic glass dissolution: II. An experimental study of the dissolution rates of basaltic glass as a function of pH and temperature. *Geochim. Cosmochim. Acta* **2003**, *67*, 3817–3832. [[CrossRef](#)]
70. Flaathen, T.K.; Gislason, S.R.; Oelkers, E.H. The effect of aqueous sulphate on basaltic glass dissolution rates. *Chem. Geol.* **2010**, *277*, 345–354. [[CrossRef](#)]
71. Stockmann, G.J.; Shirokova, L.S.; Pokrovsky, O.S.; Bénézeth, P.; Bovet, N.; Gislason, S.R.; Oelkers, E.H. Does the presence of heterotrophic bacterium *Pseudomonas reactans* affect basaltic glass dissolution rates? *Chem. Geol.* **2012**, *296–297*, 1–18. [[CrossRef](#)]
72. Prikryl, J.; Jha, D.; Stefansson, A.; Stipp, S.L.S. Mineral dissolution in porous media: An experimental and modelling study on kinetics, porosity and surface area evolution. *Appl. Geochem.* **2017**, *87*, 57–70. [[CrossRef](#)]
73. Saetre, C.; Hellevang, H.; Riu, L.; Dypvik, H.; Pilorget, C.; Poulet, F.; Werner, S.C. Experimental hydrothermal alteration of basaltic glass with relevance to Mars. *Meteorit. Planet. Sci.* **2018**, *54*, 357–378. [[CrossRef](#)]
74. Clark, D.E.; Galeczka, I.M.; Dideriksen, K.; Voigt, M.J.; Wolff-Boenisch, D.; Gislason, S.R. Experimental observations of CO<sub>2</sub>-water-basaltic glass interaction in a large column reactor experimental 50 °C. *Int. J. Greenh. Gas Control* **2019**, *89*, 9–19. [[CrossRef](#)]
75. Ralston, S.J.; Peretyazhko, T.S.; Sutter, B.; Ming, D.W.; Morris, R.V.; Garcia, A.; Ostwald, A. Phyllosilicate formation on early Mars via open-system acid alteration of basaltic glass. *Earth Planet. Sci. Lett.* **2023**, *603*, 117987. [[CrossRef](#)]
76. Kristmannsdóttir, H. Anorthosite inclusions in tertiary dolerite from the island groups Hrapppsey and Purkey, West Iceland. *J. Geol.* **1971**, *79*, 741–748. [[CrossRef](#)]
77. Saldi, G.D.; Schott, J.; Pokrovsky, O.S.; Oelkers, E.H. An experimental study of magnesite dissolution rates at neutral to alkaline conditions and 150 and 200 °C as a function of pH, total dissolved carbonate concentration, and chemical affinity. *Geochim. Cosmochim. Acta* **2010**, *74*, 6344–6356. [[CrossRef](#)]
78. Oelkers, E.H.; Golubev, S.V.; Pokrovsky, O.S.; Bénézeth, P. Do organic ligands affect calcite dissolution rates? *Geochim. Cosmochim. Acta* **2011**, *75*, 1799–1813. [[CrossRef](#)]
79. Brantley, S.L. Reaction Kinetics of Primary Rock-forming Minerals under Ambient Conditions. *Treatise Geochem.* **2003**, *5*, 605.
80. Heřmanská, M.; Voigt, M.J.; Marieni, C.; Declercq, J.; Oelkers, E.H. A comprehensive and internally consistent mineral dissolution rate database: Part I: Primary silicate minerals and glasses. *Chem. Geol.* **2022**, *597*, 120807. [[CrossRef](#)]

81. Oxburgh, R.; Drever, J.I.; Sun, Y.-T. Mechanism of plagioclase dissolution in acid solution at 25 °C. *Geochim. Cosmochim. Acta* **1994**, *58*, 661–669.
82. Icenhower, J.P.; Dove, P.M. Solution kinetic effects of amorphous silica into sodium chloride solutions: Effects of temperature and ionic strength. *Geochim. Cosmochim. Acta* **2000**, *64*, 4193–4203. [[CrossRef](#)]
83. Brady, P.V.; Walther, J.V. Kinetics of quartz dissolution at low temperatures. *Chem. Geol.* **1990**, *82*, 253–264. [[CrossRef](#)]

**Disclaimer/Publisher’s Note:** The statements, opinions and data contained in all publications are solely those of the individual author(s) and contributor(s) and not of MDPI and/or the editor(s). MDPI and/or the editor(s) disclaim responsibility for any injury to people or property resulting from any ideas, methods, instructions or products referred to in the content.